Macromolecules

Article

pubs.acs.org/Macromolecules

Self-Assembled Structures of PMAA–PMMA Block Copolymers: Synthesis, Characterization, and Self-Consistent Field Computations

Feng Li,[†] Mike Schellekens,*[,‡] Jens de Bont,[‡] Ron Peters,[‡] Ad Overbeek,[‡] Frans A. M. Leermakers,[§] and Remco Tuinier*[,∥,†]

[†]DSM ChemTech R&D, PO Box 18, 6160 MD Geleen, The Netherlands

[‡]DSM Coating Resins, Sluisweg 12, 5145 PE Waalwijk, The Netherlands

[§]Laboratory of Physical Chemistry and Colloid Science, Wageningen University, Dreijenplein 6, 6703 HB Wageningen, The Netherlands

[∥]Van 't Hoff laboratory for Physical and Colloid Chemistry, Department of Chemistry, Debye Institute, Utrecht University, Padualaan 8, 3584 CH Utrecht, The Netherlands

Supporting Information

ABSTRACT: Block copolymers composed of methacrylic acid (MAA) and methyl methacrylate (MMA) blocks are interesting candidates for replacing surfactants in emulsion polymerization methods. Here the synthesis and experimental characterization of well-defined PMAA–PMMA block copolymers made via RAFT polymerization are reported. It is shown that these block copolymers self-organize in water into micellar spherical or cylindrical structures or into highly size disperse structures (probably vesicles) in aqueous salt solutions upon increasing the pH. The physical properties of the polymer dispersions depend on the self-organization morphology which is determined by the diblock copolymer PMAA and PMMA block lengths. The relation between diblock copolymer block lengths and the self-organized structures is rationalized using self-consistent field theory (SCFT). Theoretically predicted self-assembled structures of MAA_x–MMA_y block copolymers are compared with the results obtained from experiments. Size and morphology of the self-assembled structures are in good agreement with SCFT.

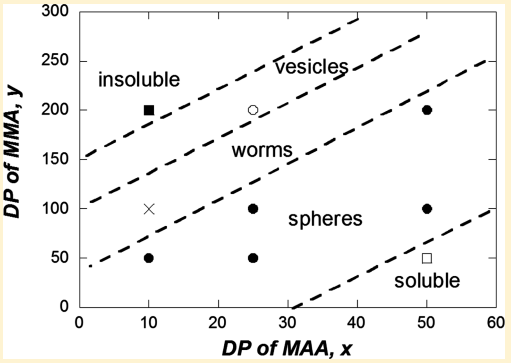

INTRODUCTION

For many years emulsion polymerization has been the most widely applied industrial process for the preparation of waterborne vinyl polymers. The method was explored first about a century ago, and first successful theories were published in the 1940s.[1,2] In particular, compared to solvent-based polymerization processes, emulsion polymerization is an inherently safer and more sustainable process. Emulsion polymerization offers many advantages such as the ability to prepare a broad range of high molar mass polymers at high reaction rate and monomer conversion while maintaining low viscosity and excellent heat dissipation. The waterborne polymer dispersions which are the end-products of an emulsion polymerization can be directly used in a multitude of applications including coatings, inks, and adhesives. The main disadvantage of emulsion polymerization is however that it relies on the use of surfactants for particle nucleation and stabilization, which remain in the end-product and can have a detrimental impact on key product performance aspects such as adhesion and water sensitivity.

An interesting alternative approach is to use nonmigrating polymeric surfactants as stabilizers in the emulsion polymerization process.[3,4] In particular, the use of amphiphilic block copolymers containing a polyelectrolyte block and a hydrophobic block has gained considerable attention in the past two decades.[5−9] Amphiphilic block copolymers offer excellent colloidal stabilization without the negative migration effects of low molar mass surfactants[10] and can furthermore provide a substantial contribution to the final emulsion polymer performance in coating applications. For example, Moñuz-Bonilla et al.[11] reported the preparation of polystyrene films with antifouling properties obtained from emulsion polymers stabilized by PEG-based amphiphilic block copolymers. Kimerling and Bhatia[12] investigated the use of acrylic acid-based amphiphilic block copolymers in waterborne coatings on cedar wood for improved tannin bleed resistance. Another example concerns coating adhesion to untreated polypropylene-based plastics obtained via controlled incorporation of selected adhering functional groups in an amphiphilic block copolymer supported emulsion polymer.[13]

In recent years the interest in using controlled radical polymerization techniques for block copolymer synthesis has

Received: September 11, 2014
Revised: December 11, 2014
Published: January 30, 2015

DOI: 10.1021/ma501878n
Macromolecules 2015, 48, 1194−1203

grown significantly from an academic as well as industrial perspective.[14] Reversible addition−fragmentation chain transfer (RAFT) polymerization in particular is one of the most suitable polymerization methodologies when it concerns the direct synthesis of a broad range of acid-based block copolymers via free-radical means.[15,16] One of the more interesting block copolymers is an amphiphilic block copolymer prepared from readily available and industrially relevant monomers like methacrylic acid (MAA) and methyl methacrylate (MMA). In order to use these block copolymers effectively as particle stabilizers in an emulsion polymerization process, however, more understanding is needed on the self-assembly behavior in water with respect to self-assembly morphology and size as a function of the block lengths, pH, and ionic strength.

Amphiphilic block copolymers in selective solvents are known to self-assemble into various geometries such as vesicles,[17−20] rodlike or cylindrical micelles,[21] small disks,[22] and spherical micelles.[23] Control over the relation between copolymer composition and self-organization morphology allows tailoring the physical properties of the polymer dispersions,[24] see also the theoretical work by Zhulina and Borisov (reviewed in refs 25 and 26) on the equilibrium structures of self-organized solvophobic/solvophilic ionic and nonionic block copolymers. For ionic copolymers such as the PMAA−PMMA copolymers studied here, there are only limited analytical results for special limits. Therefore, we use numerical self-consistent field lattice computations in this study. In aqueous salt solutions the amphiphilic nature of PMAA−PMMA block copolymers implies that self-assembly of ionized PMAA−PMMA block copolymer chains will depend on the relative block lengths of the PMAA and PMMA blocks and the polymer molar mass. A plethora of resulting self-assembled structures exists.[27] For sufficiency long PMAA blocks there is a possibility to form micellar spherical aggregates consisting of dense cores of the water-insoluble PMMA blocks and diffuse shells (coronas) formed from the water-soluble ionized PMAA blocks. Although the micellization of acid-based block copolymers in aqueous media has been studied before,[28] studies on self-assembly behavior of well-defined PMAA−PMMA block copolymers in water are limited thus far. Liu et al.[29] investigated the use of PMAA−PMMA block copolymers with varying block lengths prepared by living anionic polymerization as dispersants in a microemulsion-like polymerization with static and dynamic light scattering. Studies have also been reported on the association behavior of ATRP-derived PMAA−PMMA block copolymers in aqueous solution at various degrees of neutralization.[30,31] Zhao et al.[32] investigated the effect of chain topology of ATRP-derived copolymers of MAA and MMA with respect to pH-responsive properties and micelle formation in aqueous solution.

In this paper the synthesis and characterization of RAFT polymerized PMAA−PMMA block copolymers and the use of self-consistent field theory (SCFT) to compute the self-assembly behavior in aqueous solution are reported. SCFT is a suitable, fast, and accurate method for studying self- and coassembling systems. For example, it allows to predict the thermodynamic stability and structure of micelles from weakly charged block copolymers.[33] Both short-range solvency interactions and longer ranged electrostatic interaction are taken into account in this study. As a result, insight into the details of the equilibrium self-assembled architectures is obtained. Theoretically predicted self-assembled structures of MAA_x−MMA_y block copolymers are compared with the results obtained from experiments, where results from light scattering techniques and microscopy are presented. In future work we intend to report a study on exploring the use of these well-defined PMAA−PMMA block copolymers in emulsion polymerization.

THEORY

Self-Consistent Field Theory. Here the self-consistent field theory (SCFT) for (polymeric) self- and coassembly is briefly outlined. We use the numerical lattice approach of Scheutjens and Fleer[34,35] and apply this to a molecularly detailed model, wherein the segments in the polymer chain are described on a united-atom level (the united atoms are referred to as segments below) and the polymer chains are described via the freely jointed chain model.[36,37] SCFT has been extensively discussed in the literature before (see refs 38−41 for details). In the Scheutjens−Fleer method adopted here space is represented by a set of lattice sites. When focusing for instance on the spherical or cylindrical geometries used in this study, space is defined by a radial coordinate with lattice layers numbered $r = 0, 1, 2, ...$, where $r = 0$ coincides with the center of mass of the object. Each layer has $L(r)$ sites, and the volume fraction is found by the fraction of sites used by a particular segment type, i.e.. $\varphi_X(r) = n_X(r)/L(r)$, with n_X being the number of sites filled by segment type X. In SCFT theory, the mean-field Helmholtz free energy F is a function of volume fraction (dimensionless concentration) $\varphi(r)$ and the corresponding segment potential $u(r)$:

$$F[\{\varphi\}, \{u\}, \alpha] = -\ln Q([\{u\}]) - \sum_r L(r) \sum_X u_X(r)\varphi_X(r) + F^{\text{int}}([\{\varphi\}]) + \sum_r \alpha(r)(L(r) \sum_X \varphi_X(r) - 1) \quad (1)$$

It is noted that here and below all energies are normalized by the thermal energy k_BT. The subscript X refers to component X in the system. The first term of eq 1 represents the partition function $Q(\{u\},V,T)$ for the "potential" ensemble; that is, it can be computed when the potentials are known. The second term in eq 1 is a Legendre transformation to set the result in the normal N,V,T ensemble. The third term in eq 1 is the contribution from interactions between the different compounds, including electrostatic interactions. The solvency effects are approximated by short-range nearest-neighbor interactions by using the Bragg−Williams mean field approximation.[42] More information can be found for instance in refs 43−45. The last term of eq 1 imposes the incompressibility constraint $\sum_X \varphi_X(r) = 1$, implemented locally at each position r. This term contains a Lagrange parameter $\alpha(r)$.

Optimization of the free energy provides the constraint

$$\frac{\partial F}{\partial \varphi_X(r)} = 0 \quad (2)$$

or more specifically

$$u_X(r) = \alpha(r) + \frac{\partial F^{\text{int}}}{\partial \varphi_X(r)} \quad (3)$$

which enables to compute the self-consistent solutions of eq 1. The local potential $u_X(r)$ is the result of a combined contribution of the Lagrange field $\alpha(r)$ and the derivative of

DOI: 10.1021/ma501878n
Macromolecules 2015, 48, 1194−1203

the interaction. For details we refer to ref 33. It turns out that the grand potential Ω is the characteristic function that is relevant to determine the equilibrium structure of a given self-assembled structure. Closed expressions in terms of the segment volume fraction and segment potentials are available to evaluate the grand potential accurately. The grand potential can be obtained by subtracting the chemical potentials μ_i of all molecules i from the Helmholtz free energy, $\Omega = F - \sum_i \mu_i n_i$. The chemical potentials can be evaluated from knowledge of the composition of the bulk, φ_i^b. Here the bulk is the (water rich) phase that exists far away from the particle. For each self-assembled structure (vesicle, bilayer, spherical micelle, cylindrical micelle) a suitable lattice geometry is required. The self-assembled structure with the lowest chemical potential of the copolymers in the bulk is the preferred copolymer self-assembled structure.

Model and the Parameters. The chemical sequence of the RAFT block copolymer MAA_x–MMA_y is depicted in Figure 1 together with the related coarse-grained sequence used in this SCFT calculation. In this SCFT model all compounds are sequestered into segments. The segments are denoted as type S (water), C (representing CH_2 or CH_3), R (representing quaternary carbon or formate group), and A (representing a carboxylic acid group).

The set of Flory–Huggins χ parameters that were employed in this study is presented in Table 1. The values chosen were inspired by earlier (surfactant) micellization studies.[33,38,41] A negative value for a χ parameter indicates attractive interactions between two compounds, whereas positive values for χ parameters indicate repulsive interactions. Interactions with the solvent were chosen such that polar groups have a small or negative χ, whereas the apolar ones have a large positive value as detailed below; the solvency becomes better with decreasing χ. While the accuracy of the χ-parameter can in principle be improved using additional experiments or atomic modeling, the χ-parameters used here provide a sufficient estimation for micelle formation.[33]

In this work, pH and ionic strength need to be defined as the input for calculation, for which the bulk volume fraction of the component equals the requested value (semiopen system). It is important to note that the electrolyte volume fraction φ is a dimensionless concentration. For the conversion to molar concentration one needs the characteristic dimension of a lattice site. Here a value of 0.5 nm is used for the lattice size. Using this $\varphi_{salt}^b = 0.0008$ equals approximately 10 mM of salt concentration, and a similar conversion allows us to evaluate the pH from the volume fraction of protons.[45] The carboxylic group A dissociates with corresponding operational dissociation constant $p\tilde{K}_a = 5.52$, i.e., $pK_a = 4.25$ (in usual concentration units). It can exist in two possible states, with or without charge, with the valence value $\nu_{COO-} = -1$ and $\nu_{COOH} = 0$, respectively. The relative permittivity ϵ_A of this group is set to be equal to 10. The other components in the polymer have zero

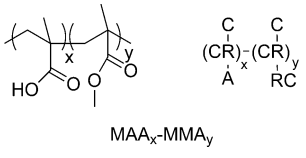

MAA_x-MMA_y

Figure 1. Chemical structure of RAFT block copolymer MAA_x–MMA_y and its related coarse-grained sequence used in this SCFT calculation.

Table 1. List of Flory–Huggins Interaction Parameters Used in the Model

χ	S	C	R	A
S	0	1.6	2.3	−0.7
C	1.6	0	0.6	1.6
R	2.3	0.6	0	2.3
A	−0.7	1.6	2.3	0

valence. Each salt ion of 1:1 electrolyte is modeled as a monomer with valence $\nu_{s+} = 1$ and $\nu_{s-} = -1$. The relative permittivities for both ions are set equal to 10. Water is modeled as a monomer with $pK_w = 14$ ($p\tilde{K}_w = 14.25$). It exists in three possible states with corresponding valence $\nu_{OH-} = -1$, $\nu_{H_2O} = 0$, and $\nu_{H_3O+} = 1$. The relative permittivity of water is equal to 80. All calculations described in this work were performed at pH 8 and at a ionic strength of 1 mM. This is also comparable with the experimental conditions.

MATERIALS, METHODS, AND CHARACTERIZATION

Block Copolymer Synthesis. All materials (MAA (Lucite International), MMA (Dow Chemicals), Perkadox AMBN (2,2-azobis(2-methylbutyronitrile), Akzo Nobel) were used as received. RAFT agent 4-cyano-4-[(dodecylsulfanylthiocarbonyl)sulfanyl]-pentanoic acid was kindly provided by CSIRO Australia and used as received. Three PMAA precursor blocks were synthesized with a target degree of polymerization (DP) of 10, 25, and 50. The synthesis of the PMAA precursor block with target DP 10 was performed as follows: 166.4 g of ethanol and 55.5 g (137 mmol) of RAFT agent were added to a 1 L flask equipped with condenser cooler, temperature measuring probe, and mechanical stirring device. The reaction mixture was degassed by purging with nitrogen at ambient temperature for 20 min while stirring. The temperature was then raised to 65 °C, and 30 vol % of a monomer feed mixture of 118.2 g (1.37 mol) of MAA and 118.2 g of ethanol was added to the reaction mixture. The reaction mixture was further heated to 75 °C followed by addition of a mixture of 1.3 g (6.8 mmol) of AMBN and 40.4 g of methyl ethyl ketone. After the reaction mixture was kept for 10 min at 75 °C the gradual addition was started of the remaining 70 vol % of the monomer feed mixture. The addition lasted 2 h under a nitrogen atmosphere and at a controlled temperature of 75 °C, after which the mixture was kept for 10 h at 75 °C. The reaction mixture was then cooled to 20 °C, and a sample was withdrawn for further analysis. The conversion of MAA as determined with liquid chromatography was 95.8 wt % and the solids mass % was found to be 37.1 wt %. The solids content of the PMAA and PMAA–PMMA polymers was determined using a Mettler Toledo HR73 Halogen moisture analyzer at 130 °C. SEC analysis resulted in the following values: M_n = 2380 g/mol, dispersity (= M_w/M_n) = 1.12 (calibration on PMMA standards). The PMAA precursor blocks with DP 25 and 50 were prepared using a similar recipe and procedure with adjustment of the molar ratio of MAA monomer to RAFT agent. The obtained PMAA precursor blocks of target DP 10, 25, and 50 were subsequently used to prepare PMAA–PMMA block copolymer with a target DP for the PMMA block of 50, 100, and 180. For the higher molar mass polymers some additional solvent (either ethanol or methyl ethyl ketone) was added during synthesis to maintain a suitable processing viscosity.

Analysis and Characterization of the Block Copolymers. *Determination of Monomer Conversion.* The conversion of MAA was determined using liquid chromatography (LC), while the conversion of MMA was determined using headspace gas chromatography. Details can be found in the Supporting Information.

Size Exclusion Chromatography. Molar masses were determined with size exclusion chromatography (SEC) using a Waters 2695 module equipped with a Waters 2410 refractive index detector (Waters, Milford, MA). Three PLgel MIXED-B (7.5 × 300 mm (i.d. ×

DOI: 10.1021/ma501878n
Macromolecules 2015, 48, 1194–1203

Table 2. Characterization of the PMAA−PMMA Block Copolymers, Including the Theoretical Molar Masses of the Blocks (th), the Conversions, and the Experimentally Determined Molar Masses

DP								
MAA (th)	MMA (th)	MAA (NMR)	MMA (calc)	conv x (%)	conv y (%)	M_n(th) (g/mol)	M_n(SEC) (g/mol)	M_w/M_n (SEC)
10		7		95.8		1230	2380	1.12
25		17		96.7		2490	3000	1.11
50		38		97.8		4610	3160	1.15
10	50	7	48		95.5	6010	6580	1.21
10	100	7	95		95.4	10780	10400	1.27
10	180	7	175		97.3	18420	18610	1.19
25	50	17	48		95.8	7280	9110	1.09
25	100	17	96		95.5	12050	13730	1.12
50	100	38	99		98.8	14510	14720	1.14

L), dp 10 μm) in series with MIXED guard column (7.5 × 50 mm (i.d × L), dp 10 μm) were used (Agilent, Avondale, PA). The flow rate was 1 mL/min, and the temperature of the column was 40 ± 1 °C. Tetrahydrofuran (THF), containing 1% (v/v) acetic acid (Biosolve BV, The Netherlands), was used as solvent, and the samples were dissolved completely; the sample concentration was 10 mg/mL, and the injection volume was 50 μL. PMMA polymer standards (Polymer laboratories, Agilent) were used for the calibration.

Gradient Liquid Chromatography. Gradient liquid chromatography separates molecules on the basis of their polarity and hence chemical composition.[46] By applying a water/THF gradient, polar molecules elute first and apolar molecules elute later. Gradient liquid chromatography was performed on a Waters 2695 module equipped with a Waters 2998 PDA detector and a Dionex Corona CAD detector. A Waters Symmetry C18 column (150 × 4.6 mm, 3.5 μm particles) was used. The concentration of the samples was 25 mg/mL, and the injection volume was 10 μL. The column temperature was 40 ± 1 °C. The flow rate was 0.5 mL/min. Chromatograms and further details can be found in the Supporting Information.

NMR Spectroscopy. ^{13}C NMR was performed to determine the average degree of polymerization and the degree of block copolymer formation as average sequence distribution of both MAA and MMA in the block copolymer samples. The measurements were done using a 400 MHz ^{13}C NMR Bruker Avance (Bruker Corporation, Billerica, MA). The samples were dissolved in pyridine (Biosolve), ±110 mg/mL pyridine, with a small amount of D_2O added for locking and shimming.

Characterization of the Polymer Dispersions. *Sample Preparation.* The block copolymer dispersions were prepared in the following way. The polymers made were first diluted with methyl ethyl ketone to a concentration of 10 wt %. Subsequently, KOH (15 wt % in water) was added at a stoichiometric ratio of 0.9 to MAA groups, corresponding to pH 8. This solution was kept as stock solution. Stable dispersions of typically 0.1 wt % final solids were made by dropwise addition of the block copolymer stock solution into 1 mM KCl water while stirring at ambient temperature. The amount of solvent volume used was kept at minimum. Samples were always kept overnight before performing light scattering experiments to reach equilibrium. Samples used for cryo-TEM were kept several days at room temperature before measuring these.

The critical micelle concentration (CMC) of the block copolymers was not measured. This would require special efforts since the CMC value is very small for polymers with relatively long hydrophobic blocks.[47−49] According to our SCFT results, the CMC of these block copolymers is extremely low. The polymers studied have a relatively low solubility, which indicates the CMC values should be low and at least well below the applied concentration of 0.1 wt %.[31]

Dynamic and Static Light Scattering. Dynamic light scattering (DLS) and static light scattering (SLS) were carried out on an ALV/DLS-5000 light-scattering apparatus (ALV, Langen, Germany), equipped with an argon ion laser (LEXEL, Palo Alto, CA) operating at a wavelength of 514.5 nm. All experiments were performed at scattering angles between 24° and 140°. Temperature was controlled at 25 °C by using a Haake C35 thermostat. From the DLS measurements one can deduce the self-diffusion coefficient of the self-assembled structures from which the hydrodynamic diameter d_h can be computed (see Supporting Information). The scattering angle plus concentration dependence of the scattered intensity from SLS provides the radius of gyration R_g and the weight-averaged particle mass M_w of the particles as well as the second osmotic virial coefficient B_2 that reflects the particle interactions (see Supporting Information).

Cryo-Transmission Electron Microscopy. A few microliters of sample was placed on a holey carbon film supported on a cryo-transmission electron microscopy (cryo-TEM) grid. A filter paper was then used to blot the drop and create a thin film. This sample was cryo-fixed by rapidly immersing into liquid ethane cooled to −170 to −180 °C. The specimen was inserted into a cryo-transfer holder and then transferred to a JEOL JEM2100 TEM. Examinations were carried out at temperatures around −170 °C. The TEM was operated at an acceleration voltage of 200 kV. Zero-loss filtered images were taken under low dose conditions (1000−2000 nm^2).

RESULTS AND DISCUSSION

In Table 2 an overview is given of the characterization data as determined for the prepared PMAA precursor blocks and the PMAA−PMMA block copolymers. Theoretical molar masses were calculated from the equation

$$M_n = \frac{x[\mathrm{MAA}]M_{\mathrm{MAA}}}{[\mathrm{RAFT}]} + \frac{y[\mathrm{MMA}]M_{\mathrm{MMA}}}{[\mathrm{RAFT}]} + M_{\mathrm{RAFT}}$$

where M_n is the number-average molar mass, M_{MAA}, M_{MMA}, and M_{RAFT} are the molar masses of MAA, MMA, and RAFT agent, [MAA], [MMA], and [RAFT] are the molar concentrations of MAA, MMA, and RAFT agent, and x and y are the fractional conversions of MAA and of MMA, respectively. High monomer conversion levels were obtained which allowed the synthesized PMAA precursor blocks to be used directly for chain extension with MMA without the need for purification.

The results in Table 2 show that the M_n values of the PMAA−PMMA block copolymers as determined from SEC analyses are in good agreement with the theoretical M_n values and that the dispersity values are all low, which is indicative for good polymerization control. Furthermore, the degree of block copolymer formation as determined with ^{13}C NMR is above 96% for all synthesized block copolymers. For the three PMAA precursor blocks, however, a deviation is seen between the theoretically predicted M_n values and the M_n values as determined from SEC analysis. This deviation could be partially explained from the fact the calibration was performed on PMMA standards. Similar type of deviations in experimental versus theoretical M_n values of low molar mass (M_n < 4000 g/mol) RAFT-derived PMAA chains have however been reported

DOI: 10.1021/ma501878n
Macromolecules 2015, 48, 1194−1203

by Chaduc et al.,[50] who studied the RAFT polymerization of MAA in water using a similar type of cyanotrithiocarbonate RAFT agent, namely 4-cyano-4-thiothiopropylsulfanyl-pentanoic acid. They reported that the deviation is most probably due to a rather low chain transfer ability of the applied RAFT agent in MAA polymerization, which basically means that it will take up to a certain level of MAA conversion before the RAFT agent is converted to PMAA-RAFT species. In order to understand the implication of the deviation of the experimental versus theoretical M_n values gradient, LC analyses were performed on the synthesized PMAA precursor blocks. The maximum UV absorbance for the characteristic C═S bond of the applied trithiocarbonate RAFT agent was measured at 310 nm. Combination of a UV detector at 310 nm, which shows the number distribution of chains bearing the trithiocarbonate end-group, with a CAD detector, which shows the mass distribution of all polymer chains, therefore made it possible to differentiate between polymer chains that bear a trithiocarbonate end-group and those that do not. For all three PMAA blocks the CAD chromatogram shows a major peak at 29 min, which also appears in the UV chromatogram at 310 nm, and a smaller peak in the range of 22−28 min, which does not appear in the UV chromatogram at λ = 310 nm (see Figure S1 in the Supporting Information). The major UV-absorbing peak is assigned to the target PMAA-RAFT chains whereas the secondary non-UV-absorbing peak represents PMAA chains that do not bear the hydrophobic dodecyl-trithiocarbonate end-group. Formation of this fraction of non-RAFT functional PMAA chains might be related to a low chain transfer ability of the RAFT agent in MAA polymerization combined with the low target molar mass but might also be (partially) related to chain transfer reactions to solvent (ethanol). Because of the formation of non-RAFT functional PMAA, the actual average DP values of the PMAA blocks that are part of the PMAA−PMMA block copolymers will be lower than expected. For an optimal comparison to the SCFT calculations reliable data are required on the average degree of polymerization. In order to obtain a more accurate estimation of the average DP values of the PMAA-RAFT blocks, the block copolymers were purified from non-RAFT functional PMAA polymer and subsequently analyzed with ^{13}C NMR. Thereto, the final PMAA−PMMA block copolymers with target DP 10−100 and 25−100 were precipitated in a 50:50 vol % methanol:water mixture to remove excess of non-RAFT functional PMAA material. The PMAA−PMMA block copolymer with target DP 50−100 was precipitated in demineralized water. Precipitation was performed three times, where after the first and second precipitation step the precipitated samples were dried under vacuum at 50 °C and redissolved in THF. Confirmation was obtained from LC analysis that the non-RAFT functional PMAA was effectively removed from the purified block copolymer samples (see Figure S2 in the Supporting Information). The purified samples were subsequently analyzed with ^{13}C NMR to determine the degree of polymerization of the PMAA block by comparing the quaternary C integral of the MMA block versus that of the MAA block. The degree of polymerization of the MMA block was determined from the theoretical DP MMA value, corrected by the MMA conversion y as determined by gas chromatography analysis. It is noted that the purification was solely performed for analysis purposes. Later characterizations of the synthesized polymers and self-assembled structures were performed on unpurified block copolymers. The presence of non-RAFT functional PMAA is not expected to impact the measurements as it will be fully dissolved in the (dilute) aqueous phase.

Before performing SCFT calculations, the lattice geometry needs to be defined. In a spherical lattice, one can evaluate the thermodynamic stability of spherical micelles or spherical vesicles. A cylindrical lattice geometry allows to study cylindrical or wormlike micelles (end-effects are then typically ignored). Moreover, a flat lattice is used to consider the stability of planar bilayers. Using the SCFT machinery, it is possible to generate for a given system the thermodynamically possible types of self-assembled systems. In general, the chemical potentials of the amphiphiles in these self-assembled systems, which are termed aggregates here, is a function of the lattice geometry used. The association type for which the molecules have the lowest chemical potential is the preferred one.

We determined the chemical potentials of self-assembled wormlike micelles, spherical micelles, and flat bilayers under thermodynamic equilibrium conditions (at which the grand potential Ω equals zero) at various chemical compositions using SCFT. The morphology with the lowest chemical potential corresponds to the thermodynamically most preferred self-assembled objects. By doing this, we were able to compute the phase diagram of MAA_x−MMA_y RAFT diblock copolymers as a function of the chain lengths (degree of polymerization DP) of the two building blocks x and y, and the result is shown in Figure 2. By varying the chain lengths of the blocks, the assembly behavior of the RAFT block copolymers in water can change from completely soluble toward a preferred spherical micelle structure, a preferred wormlike micelle, or a vesicle upon increasing the relative hydrophobicity. When the diblock copolymers become too hydrophobic, they cannot be dispersed in water anymore.

In this paper, two well-defined block copolymers made via the RAFT synthesis method will be discussed in more detail. These are MAA_7−MMA_{48} and MAA_7−MMA_{95}. As shown in the theoretical phase diagram drawn in Figure 2, MAA_7−MMA_{48} copolymers are expected to form spherical micelles. The grand potential of the diblock copolymer as a function of micelle aggregation number is plotted in Figure 3.

The grand potential Ω, the free energy of formation of a single micelle, is computed as a function of the aggregation number g. In Figure 3a it is shown that the grand potential of

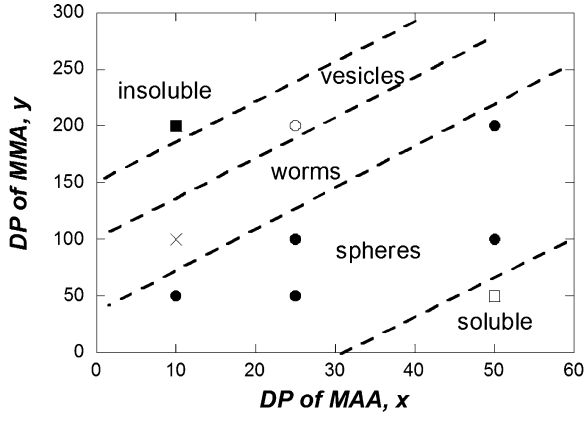

Figure 2. Theoretical phase diagram of dilute MAA_x−MMA_y block copolymers in aqueous salt solution of 1 mM KCl at pH 8 from numerical SCFT lattice computations. The regions for the different self-organized structures are indicated.

DOI: 10.1021/ma501878n
Macromolecules 2015, 48, 1194−1203

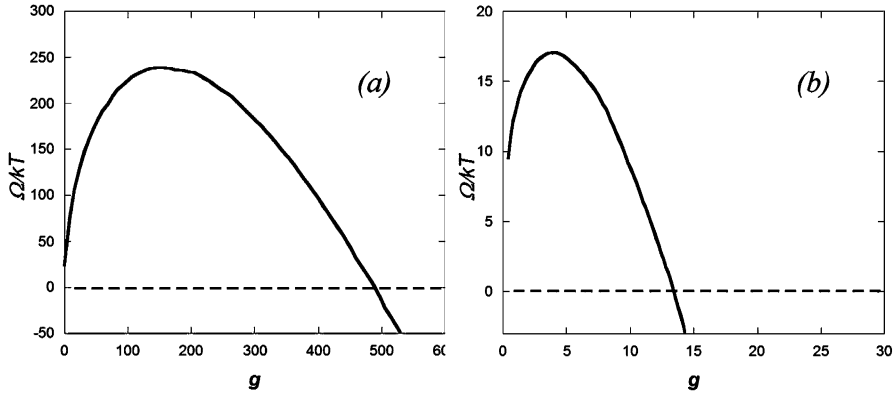

Figure 3. Grand potential Ω of self-assembled structures of PMAA−PMMA block copolymers in aqueous solutions for (a) a micelle composed of block copolymers MAA_7−MMA_{48} in spherical geometry and for (b) a micelle made of block copolymer MAA_7−MMA_{95} in cylindrical geometry.

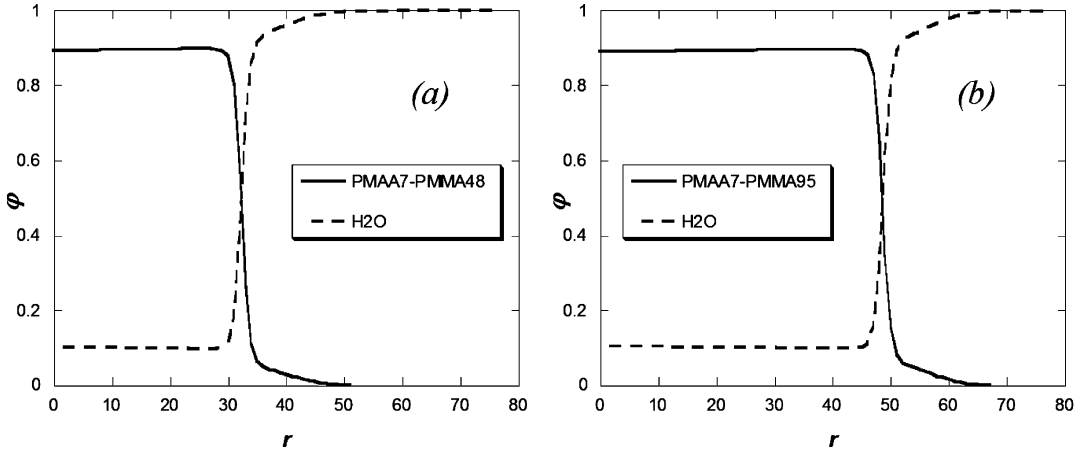

Figure 4. SCFT volume fraction profiles: (a) density profiles of block copolymers MAA_7−MMA_{48} and water in a spherical geometry; (b) density profile of block copolymers MAA_7−MMA_{95} in cylindrical geometry. Block copolymer and water lattice volume fractions are plotted as a function of the distance r (in lattice units) from the center of the geometry.

this system increases first with increasing g, reaches a maximum, and then has a negative slope $\partial\Omega/\partial g < 0$ for larger values of g, which is the characteristic for stable micelles. A relevant point on this curve is the condition where the free energy of forming a micelle attains the value $\Omega = 0$. This micelle then corresponds to an equilibrium micelle under the assumption that the translational entropy of the micelles can be ignored. For this selected micelle the aggregation number is $g \approx 480$. Furthermore, we depicted the SCFT density profiles of block copolymers and water as a function of the radial distance from the center of a micelle (computations are performed for a cross section) in Figure 4a for MAA_7−MMA_{48} polymers for a spherical geometry (the unit is approximately 0.5 nm).

For the more hydrophobic diblock copolymers MAA_7−MMA_{95}, SCFT revealed that a wormlike micelle is the thermodynamically preferred state compared to the spherical micelle. In Figure 3b, the grand potential is plotted for MAA_7−MMA_{95} copolymers as a function of micelle aggregation number. The resulting equilibrium density profile (from $\Omega = 0$) is shown in Figure 4b. By comparing the density profiles in Figure 4, it follows that the micellar radius of the block copolymer MAA_7−MMA_{95} is larger than the micellar radius of the block copolymer MAA_7−MMA_{48}. Hence, the radius of the *cylindrical* micelles composed of MAA_7−MMA_{95} block copolymers is larger than the radius of *spherical* micelles of MAA_7−MMA_{48} polymers.

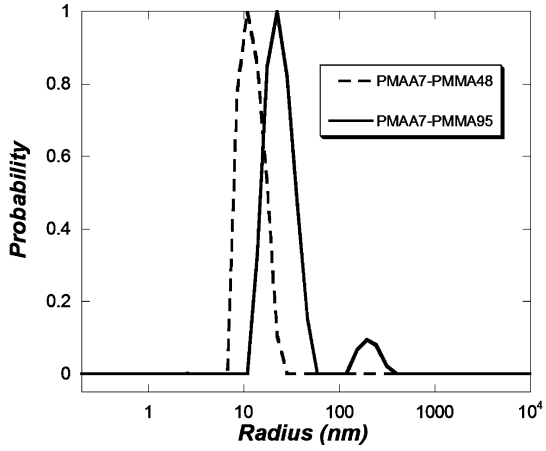

Figure 5. Particle size distributions measured using dynamic light scattering at a detection angle of 26°.

The predicted SCFT results are now compared to experimental results on the self-assembled structures. In Figure 5 the measured micelle size distributions are plotted. These were obtained from dynamic light scattering results, measured at a detection angle of 26° (where "larger" particles could also be detected). Based on the DLS result, it can be concluded that the micelle formed from MAA_7−MMA_{48} copolymers has a

DOI: 10.1021/ma501878n
Macromolecules 2015, 48, 1194−1203

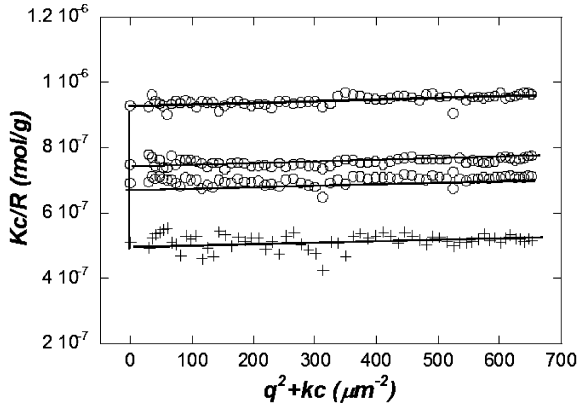

Figure 6. Zimm plot of self-assembled block copolymer MAA_7–MMA_{48} in aqueous solution using static light scattering. Concentrations of the sample from top to bottom are 0.17, 0.125, and 0.10 mg/mL. The lowest data points (plusses) correspond to the extrapolated vanishing concentration limit.

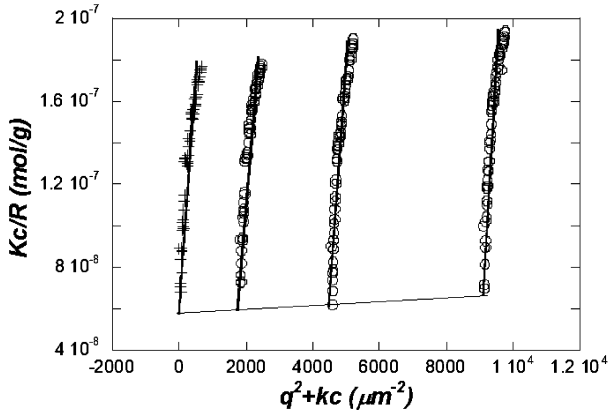

Figure 7. Zimm plot of self-assembled block copolymer MAA_7–MMA_{95} in aqueous solution using static light scattering. Concentrations of the samples from left to right are 0.10, 0.25, and 0.5 mg/mL.

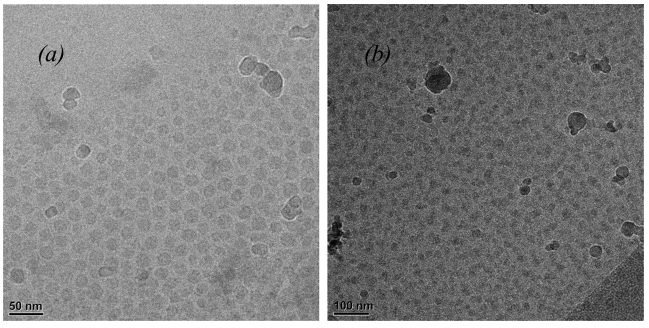

Figure 8. Cryo-TEM image of self-assembled (a) block copolymer MAA_7–MMA_{48} with spherical geometry and (b) block copolymer MAA_7–MMA_{95} with cylindrical geometry.

narrower micelle size distribution compared to the micelle formed from MAA_7–MMA_{95} copolymers. The latter one in fact exhibits a bimodal distribution of sizes with averaged hydrodynamic radii of 24.5 and 227 nm, respectively, the latter reflecting the length of the cylindrical micelles. These results are also in line with the SCFT prediction that MAA_7–MMA_{95} forms cylindrical micelles with a larger radius (24.5 nm) in comparison with the radius of spherical micelles from MAA_7–

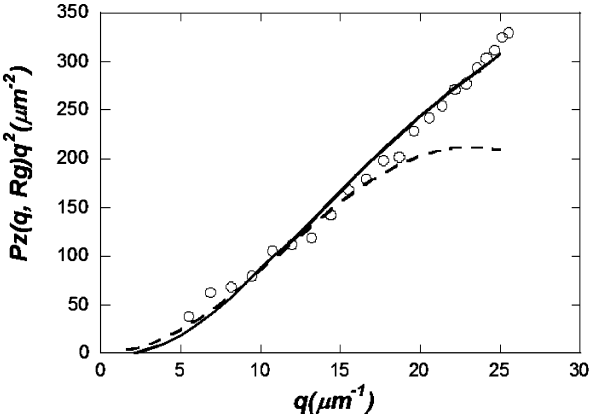

Figure 9. Particle scattering form factor of self-assembled MAA_7–MMA_{95} block copolymers in aqueous 1 mM KCl salt solution at pH 8. Open circles are experimental data points with error bars. Curves are best fits to the theoretical form factors of a thin rod (solid curve) and to the form factor a solid spherical particle (dashed curve).

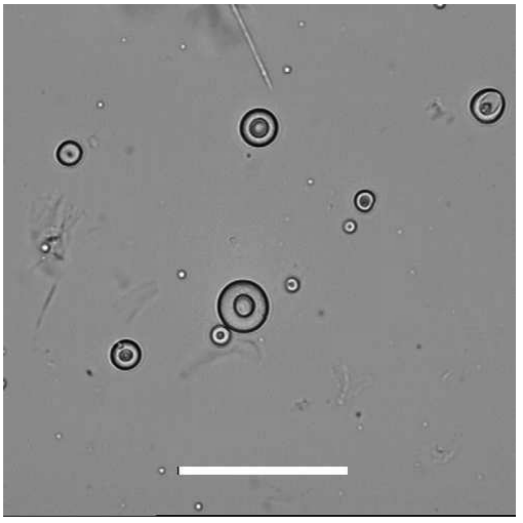

Figure 10. Light microscopy image of various multilamellar "onion"-like structures formed from self-assembling MAA_7–MMA_{175} block copolymers in aqueous 1 mM KCl at pH 8. The small and large structures shown indicate a large size dispersity. Scale bar is 50 μm.

MMA_{48} (12.5 nm). Since SCFT predicts that the MAA_7–MMA_{95} copolymers are expected to form wormlike micelles instead of spherical micelles, the first peak to the cross section may be assigned to the radius of the micelle and the second peak might correspond to the length of micelle.

Next to the DLS study, static light scattering (SLS) experiments were performed. The results are presented in terms of Zimm plots in Figures 6 and 7. Zimm plots for particles formed from MAA_7–MMA_{48} polymers are shown in Figure 6. The weight-averaged mass of the micelles is found to be 1.14×10^6 g/mol after fitting the measurements done on three concentrations. The micellar aggregation number can be calculated from the particle mass divided by the molar mass of the polymer MAA_7–MMA_{48}. This aggregation number was compared with the one from SCFT. This ends up with a number of 210, which although is smaller than 488 from SCFT prediction, has the same order of magnitude.

Although the RAFT block copolymers we studied in this paper are of relatively high purity, a small fraction of PMMA

DOI: 10.1021/ma501878n
Macromolecules 2015, 48, 1194–1203

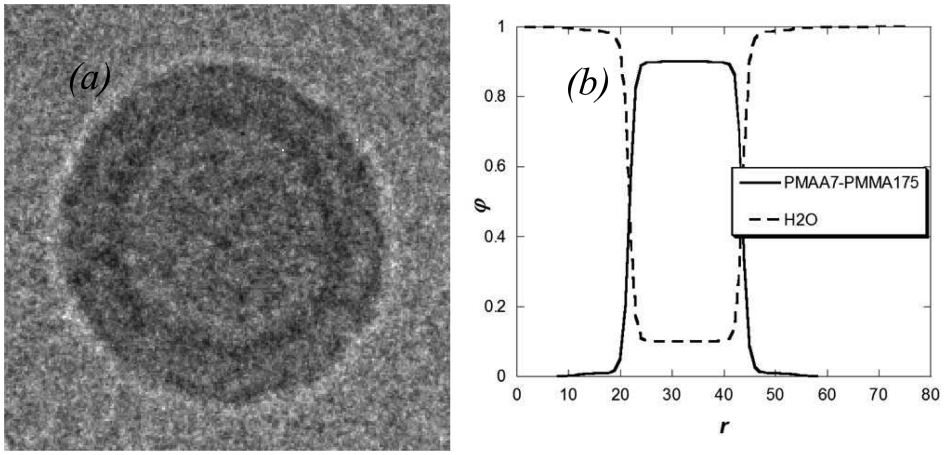

Figure 11. Particles formed from self-assembling MAA_7–MMA_{175} block copolymers: (a) cryo-TEM image (width of this image is 100 nm) and (b) SCFT density profiles for a vesicle structure of polymer and water as a function of the radial distance from the center of the vesicle.

homopolymer will most likely have been formed (inherent to RAFT synthesis). This free PMMA will be encapsulated in the core of the self-assembled structures. This influences the size a bit, but it especially changes the aggregation number (size scales with $g^{1/3}$). Besides, all measured masses of the self-organized structures have some experimental error (unavoidable when doing SLS), and the masses determined follow from fitting to a Zimm plot. It is noted that the weight-averaged aggregation number obtained from a Zimm plot derives from two extrapolations (see Supporting Information).

The same SLS study was also performed on MAA_7–MMA_{95}, and the Zimm plot is shown in Figure 7. The average molar mass of the micelle is found to be 1.43×10^7 g/mol after fitting the measurements. This number is an order of magnitude larger than the mass of the self-assembled MAA_7–MMA_{48} polymers. The aggregation number is now 1313 instead of 193, which can be explained by the SCFT result that MAA_7–MMA_{95} copolymers assemble into a cylindrical wormlike micelle structure, while MAA_7–MMA_{48} polymers assemble into a spherical micelle.

To further validate the results from both SCFT study and DLS/SLS measurements, we also performed cryo-TEM measurements on these micelles. As seen from the image of Figure 8, it is fair to say that MAA_7–MMA_{48} indeed gives a narrow size distribution of spherical micelles with a diameter close to 15 nm, which is in line with the DLS results and the SCFT predictions. Contrary to the MAA_7–MMA_{48}, the wormlike micelles composed of MAA_7–MMA_{95} in fact look polydisperse and nonspherical, as expected for such cylindrical micelles. Further, the structures from cryo-TEM look like morphologies of short wormlike micelles reported by Blanazs et al.[51] (see their Figure 5b). In order to confirm the cylindrical morphology that appears due to self-assembling MAA_7–MMA_{95} block copolymers, the scattering form factor $P(q)$ was studied as a function of the scattering vector q for a dilute sample. The resulting measured form factor from static light scattering is plotted as $q^2P(q)$ versus q in Figure 9. Comparison with theoretical fits (curves) to the form factors of a thin rod and a sphere shows that the thin rod description accurately describes the form factor. This corroborates the finding of a wormlike or cylindrical micelle structure of these self-assembling diblock copolymers.

From the theoretical phase diagram obtained from SCFT computations as shown in Figure 2 it follows that for relatively large MMA block lengths the vesicle morphology is the thermodynamically preferred structure. Hence, MAA_7–MMA_{175} block copolymers were synthesized, and dispersions of these polymers were prepared. Indeed, microscopy (see Figure 10) and TEM reveal that the dispersions seem to be composed of vesicles. A cryo-TEM picture is depicted in Figure 11a. The SCFT density profile of the polymers and solvent inside the vesicle was computed and is shown in Figure 11b. The thickness of the computed bilayer is roughly equal to 12 nm (about 24 lattice sites and each lattice site is about 0.5 nm) and corresponds to the bilayer of the particles (probably vesicles) from cryo-TEM. It is noted that the particles are highly disperse in size, which often is the case for vesicles. Several larger particles are multilamellar (see Figure 10). Further, it is likely that block lengths were chosen that are very close to the region where the PMAA–PMMA polymers get insoluble in water (see the SCFT phase diagram, Figure 2). It is possible to make vesicles with a much narrower size dispersity by mixing two types of block copolymers (see Gonzato et al.[52]).

Besides the two model polymers shown in the main text, more SLS experiments and SCFT computations were performed on self-assembling MAA_x–MMA_y polymers with several block chain lengths. Several results are summarized in Table 3. For MAA_{17}–MMA_{48}, MAA_{38}–MMA_{99}, and MAA_{17}–MMA_{96} the SCFT results for g are 20, 13, and 117, respectively. The latter value is reasonable while the first two values are too small as compared to experiments. We think our results are sensitive to solvent conditions (ionic strength) and might be sensitive to the precise dispersion method. Also, SCFT is a mean-field method which may deviate somewhat for charged systems where fluctuations are important, especially for relatively long charged blocks. The deviations between SCFT predictions and experimental data could also originate from the coarse-grained approach applied in our theoretical model, and the parameters used in SCFT can be further improved, which would require molecular simulations. In the end, however, SCFT correctly predicts the self-assembling morphology of MAA_x–MMA_y block copolymers (wormlike or spherical micelles) as well as the size of the micelles and is thus a very useful tool to rationalize the physical properties of amphiphilic charged copolymers.

DOI: 10.1021/ma501878n
Macromolecules 2015, 48, 1194–1203

Table 3. Hydrodynamic Radius from Dynamic Light Scattering and SCFT Size Prediction Plus Micelle Aggregation Number g[a]

block copolymers	morphology	R_h/nm (DLS)	R_h/nm (SCFT)	g_{SLS}
MAA_7–MMA_{48}	sphere	12.5	12.0	210 ± 74
MAA_7–MMA_{95}	cylinder	24.5/227		1313 ± 40
MAA_7–MMA_{175}	vesicle[b]	highly disperse	12 nm[c]	
MAA_{17}–MMA_{48}	sphere	12.4	13.5	96 ± 7
MAA_{17}–MMA_{96}	sphere	15.7	15.8	150 ± 3
MAA_{38}–MMA_{99}	sphere	20.0	19.8	93 ± 8

[a]The structures that are suspected to be vesicles are too disperse in size to identify an averaged size. [b]These structures seem to be vesicles. [c]Bilayer thickness.

CONCLUDING REMARKS

Well-defined PMAA–PMMA diblock copolymers of low dispersity have been prepared via RAFT polymerization. The polymers have been characterized using size exclusion chromatography, gradient liquid chromatography, and NMR. The block lengths determined by ^{13}C NMR were used as input for a theoretical study using molecularly realistic self-consistent field theory (SCFT). This enabled the calculation of the properties of self-assembled PMAA–PMMA diblock copolymers in aqueous 1 mM KCl salt solutions at pH 8. In combination with (dynamic and static) light scattering and microscopy studies, it is shown that the self-assembled spherical and cylindrical micelle structures as well as the vesicles obtained from SCFT can be rationalized. Overall, good agreement is found between experimental results for the size and morphology of the self-assembled micelles and SCFT predictions. By changing the molar masses of the PMAA and PMMA blocks, it is demonstrated that the self-assembled structures can be modified from spherical micelles toward cylindrical micelles and seemingly also to vesicles. A theoretical phase diagram with various combinations of the PMAA and PMMA block with different chain length is generated that matches with our experimental observations.

ASSOCIATED CONTENT

Supporting Information

Analysis of monomer conversion and block copolymers as well as on the characterization of the block copolymers made, including more explanation on static and dynamic light scattering. This material is available free of charge via the Internet at http://pubs.acs.org.

AUTHOR INFORMATION

Corresponding Authors

*E-mail mike.schellekens@dsm.com; fax +31 416 689922; Tel +31 416 689842R (M.S.).

*E-mail r.tuinier@uu.nl; fax +31 30 253 3870; Tel +31 30 253 2391(3) (R.T.).

Author Contributions

F.L. and M.S. contributed equally.

Notes

The authors declare no competing financial interest.

ACKNOWLEDGMENTS

We thank Jan van Lent from Wageningen University for making the cryo-TEM accessible. The authors thank CSIRO Australia for kindly providing the RAFT agent. Dr. J. G. J. L. Lebouille (DSM) is thanked for useful discussions.

REFERENCES

(1) Harkins, W. D. J. *J. Am. Chem. Soc.* **1947**, *69*, 1428.
(2) Smith, W. V.; Ewart, R. H. *J. Chem. Phys.* **1948**, *16*, 592.
(3) Napper, D. H. *Polymeric Stabilization of Colloidal Dispersions*; Academic Press: New York, 1983.
(4) Piirma, I. In *Polymeric Surfactants*; Surfactant Science Series 42; Marcel Dekker Inc.: New York, 1992; pp 127–164.
(5) Müller, H.; Leube, W.; Tauer, K.; Förster, S.; Antonietti, M. *Macromolecules* **1997**, *30*, 2288.
(6) Burguière, C.; Pascual, S.; Coutin, B.; Polton, A.; Tardi, M.; Charleux, B.; K. Matyjaszewski, K.; Vairon, J.-P. *Macromol. Symp.* **2000**, *150*, 39.
(7) Ferguson, C. J.; Hughes, R. J.; Pham, B. T. T.; Hawkett, B. S.; Gilbert, R. G.; Serelis, A. K.; Such, C. H. *Macromolecules* **2002**, *35*, 9243.
(8) Riess, G.; Labbe, C. *Macromol. Rapid Commun.* **2004**, *25*, 401.
(9) Ji, J.; Yan, L.; Xie, D. *J. Polym. Sci., Part A: Polym. Chem.* **2008**, *46*, 3098.
(10) Shirakbari, N.; Ebrahimi, M.; Salehi-Mobarakeh, H.; Khorasani, M. *J. Macromol. Sci., Part B: Phys.* **2014**, *7*, 1286–1292.
(11) Muñoz-Bonilla, A.; van Herk, A. M.; Heuts, J. P. A. *Macromolecules* **2010**, *43*, 2721.
(12) Kimerling, A. S.; Bhatia, S. R. *Prog. Org. Coat.* **2004**, *51*, 15.
(13) Schellekens, M.; Twene, D.; van der Waals, A. *Prog. Org. Coat.* **2011**, *72*, 138.
(14) Destarac, M. *Macromol. React. Eng.* **2010**, *4*, 165.
(15) Chong, Y. K.; Lee, T. P. T.; Moad, G.; Rizzardo, E.; Thang, S. H. *Macromolecules* **1999**, *32*, 2071.
(16) Gaillard, N.; Guyot, A.; Claverie, J. *J. Polym. Sci., Part A: Polym. Chem.* **2003**, *41*, 684.
(17) Discher, D. E.; Eisenberg, A. *Science* **2002**, *297*, 967.
(18) Meier, W.; Nardin, C.; Winterhalter, M. *Angew. Chem., Int. Ed.* **2000**, *39*, 4599–4602.
(19) Kita-Tokarczyk, K.; Grumelard, J.; Haefele, T.; Meier, W. *Polymer* **2005**, *46*, 3540–3563.
(20) Letchford, K.; Burt, H. *Eur. J. Pharm. Biopharm.* **2007**, *65*, 259–269.
(21) Won, Y.; Davis, H. T.; Bates, F. S. *Science* **1999**, *283*, 960.
(22) Egelhaaf, S. U.; Schurtenberger, P. *Phys. Rev. Lett.* **1999**, *82*, 2804.
(23) Li, Z.; Kesselman, E.; Talmon, Y.; Hillmyer, M. A.; Lodge, T. P. *Science* **2003**, *306*, 98.
(24) Zhang, L. F.; Eisenberg, A. *Science* **1995**, *268*, 1728–1731.
(25) Borisov, O. V.; Zhulina, E. B.; Leermakers, F. A. M.; Müller, A. H. E. *Adv. Polym. Sci.* **2011**, *241*, 57–129.
(26) Zhulina, E. B.; Borisov, O. V. *Macromolecules* **2012**, *45*, 4429–4440.
(27) Mai, Y.; Eisenberg, A. *Chem. Soc. Rev.* **2012**, *41*, 5969.
(28) Riess, G. *Prog. Polym. Sci.* **2003**, *28*, 1107.
(29) Liu, T.; Schuch, H.; Gerst, M.; Chu, B. *Macromolecules* **1999**, *32*, 6031.
(30) Ravi, P.; Wang, C.; Tam, K. C.; Gan, L. H. *Macromolecules* **2003**, *36*, 173.
(31) Yao, J.; Ravi, P.; Tam, K. C.; Gan, L. H. *Langmuir* **2004**, *20*, 2157.
(32) Zhao, Y.; Luo, Y. W.; Li, B. G.; Zhu, S. *Langmuir* **2011**, *27*, 11306.
(33) Lauw, Y.; Leermakers, F. A. M.; Cohen Stuart, M. A. *J. Phys. Chem. B* **2003**, *107*, 10912.
(34) Scheutjens, J. M. H. M.; Fleer, G. J. *J. Phys. Chem.* **1979**, *83*, 1619.
(35) Fleer, G. J.; Cohen Stuart, M. A.; Scheutjens, J. M. H. M.; Cosgrove, T.; Vincent, B. *Polymers at Interfaces*; Chapman and Hall: London, 1993.
(36) Leermakers, F. A. M.; Barneveld, P. A.; Sprakel, J.; Besseling, N. A. M. *Phys. Rev. Lett.* **2006**, *97*, 066103.

DOI: 10.1021/ma501878n
Macromolecules 2015, 48, 1194–1203

(37) Kik, R. A.; Kleijn, J. M.; Leermakers, F. A. M. *J. Phys. Chem. B* **2005**, *109*, 14251.
(38) Hurter, P. N.; Scheutjens, J. M. H. M.; Hatton, T. A. *Macromolecules* **1992**, *26*, 5592.
(39) Oversteegen, S. M.; Leermakers, F. A. M. *Phys. Rev. E* **2000**, *62*, 8453.
(40) Evers, O. A.; Scheutjens, J. M. H. M.; Fleer, G. J. *Macromolecules* **1990**, *23*, 5221.
(41) Leermakers, F. A. M.; Eriksson, J. C.; Lyklema, J. *Fundamentals of Interface and Colloid Science*; Lyklema, J., Ed.; Elsevier: Amsterdam, 2005; Vol. *V*, Chapter 4.
(42) Flory, P. *Principles of Polymer Chemistry*; Cornell University Press: Ithaca, NY, 1953.
(43) Björling, M.; Linse, P.; Karlstrom, G. *J. Phys. Chem.* **1990**, *94*, 471.
(44) Israels, R. Adsorption of Charged Diblock Copolymers: Effect on Colloidal Stability. Doctoral Thesis, Wageningen University, 1994.
(45) Van Male, J. Self-Consistent-Field Theory for Chain Molecules: Extensions, Computational Aspects, and Applications. Doctoral Thesis, Wageningen University, 2003.
(46) Cools, P. J. C. H.; Maesen, F.; Klumperman, L.; van Herk, A. M.; German, A. L. *J. Chromatogr. A* **1996**, *736*, 125.
(47) Ge, H.; Hu, Y.; Jiang, X.; Cheng, D.; Yuan, Y.; Bi, H.; Yang, C. *J. Pharm. Sci.* **2002**, *91*, 1463.
(48) Jacquin, M.; Muller, P.; Talingting-Pabalan, R.; Cottet, H.; Berret, J. F.; Futterer, T.; Théodoly, O. *J. Colloid Interface Sci.* **2007**, *316*, 897.
(49) Lamprou, A.; Xie, D.; Storti, G.; Wu, H. *Colloid Polym. Sci.* **2014**, *292*, 677−685.
(50) Chaduc, I.; Lansalot, M.; Agosto, F.; Charleux, B. *Macromolecules* **2012**, *45*, 1241.
(51) Blanazs, A.; Madsen, J.; Battaglia, G.; Ryan, A. J.; Armes, S. P. *J. Am. Chem. Soc.* **2011**, *133*, 16581.
(52) Gonzato, C.; Semsarilar, M.; Jones, E. R.; Li, F.; Krooshof, G. J. P.; Wyman, P.; Mykhaylyk, O. O.; Tuinier, R.; Armes, S. P. *J. Am. Chem. Soc.* **2014**, *136*, 11100.

DOI: 10.1021/ma501878n
Macromolecules 2015, 48, 1194−1203